IOP Publishing Superconductor Science and Technology
Supercond. Sci. Technol. 31 (2018) 045001 (11pp) https://doi.org/10.1088/1361-6668/aaa65d

Evidence for preferential flux flow at the grain boundaries of superconducting RF-quality niobium

Z-H Sung[1,2], P J Lee[1], A Gurevich[3] and D C Larbalestier[1]

[1] Applied Superconductivity Center, National High Magnetic Field Laboratory, Tallahassee, FL 32310, United States of America
[2] Technical Division, Fermi National Accelerator Laboratory, Batavia, IL 60510, United States of America
[3] Department of Physics, Old Dominion University, Norfolk, VA 23529, United States of America

E-mail: zsung@fnal.gov

Received 25 July 2017, revised 22 December 2017
Accepted for publication 9 January 2018
Published 19 February 2018

Abstract

The question of whether grain boundaries (GBs) in niobium can be responsible for lowered operating field (B_{RF}) or quality factor (Q_0) in superconducting radio frequency (SRF) cavities is still controversial. Here, we show by direct DC transport across planar GBs isolated from a slice of very large-grain SRF-quality Nb that vortices can preferentially flow along the grain boundary when the external magnetic field lies in the GB plane. However, increasing the misalignment between the GB plane and the external magnetic field vector markedly reduces preferential flux flow along the GB. Importantly, we find that preferential GB flux flow is more prominent for a buffered chemical polished than for an electropolished bi-crystal. The voltage–current characteristics of GBs are similar to those seen in low angle grain boundaries of high temperature superconductors where there is clear evidence of suppression of the superconducting order parameter at the GB. While local weakening of superconductivity at GBs in cuprates and pnictides is intrinsic, deterioration of current transparency of GBs in Nb appears to be extrinsic, since the polishing method clearly affect the local GB degradation. The dependence of preferential GB flux flow on important cavity preparation and experimental variables, particularly the final chemical treatment and the angle between the magnetic field and the GB plane, suggests two more reasons why real cavity performance can be so variable.

Keywords: superconducting radio frequency, niobium, electromagnetic transport properties, SRF Nb cavity, grain boundary

(Some figures may appear in colour only in the online journal)

1. Introduction

With the push to develop high performance superconducting radio frequency (SRF) Nb cavities, the role of grain boundaries (GBs) as potentially important RF current-limiting defects needs to be better understood. During the past few decades, the SRF technology has made big strides with some cavities now approaching the theoretical performance limits of Nb. For instance, a single cell cavity made of high purity residual resistivity ratio ((RRR) > 250), large grain (>5–10 cm) niobium ingot slice reached accelerating electric fields of 45–50 MV m^{-1} at the maximum magnetic field, H_{RF} = 150–180 mT, which is close to the theoretical superheating field, $\mathbf{B}_{sh}$, of niobium at 2 K [1–3]. However, the significant degradation of the quality factor $Q(H_{RF})$ above the RF fields of $H_{RF} \geqslant 120$ mT which have been often observed on the Nb cavities hinders the progress in reaching the maximum accelerating gradient in multi-cell cavities like those needed for the International Linear Collider (ILC). Performance loss referred to as the high-field Q slope (HFQS) is a complicated phenomenon and the mechanisms of

which in relation to intrinsic materials and superconducting properties have not been well understood [4].

Many models of HFQS have been suggested in the literature; for instance, the hydride proximity effect with vacancy-hydrogen complex formation [5–8], oxide redistribution [9, 10], preferential flux penetration induced by surface roughness combined with dislocations [11] and trapped vortex hotspots [12, 13]. Although such models generally postulate a surface with degraded superconducting properties within a London penetration depth, $\lambda \sim 50$ nm, relative to the bulk, the variation of superconducting properties within the three-dimensional (3D) GB network inevitable in any real Nb cavity has not been addressed. GBs in metallic SRF Nb are prone to segregation of impurities and other materials defects during cavity fabrication [4], which may result in the suppression of the superconducting order parameter at the grain boundary. However, the extent to which the GBs degrade the SRF cavity performance is not fully understood and remains the topic of ongoing investigation [2, 14, 15]. Previous thermometry studies of the influence of grain size on the SRF performance of the Nb cavities [16, 17] have shown that only ~10%–20% of GBs can trigger localized cavity breakdown. An optical inspection system [18] showed that some GBs found in a prototype 9 cell ILC cavity contribute to the HFQS and the cavity quench [19]. Thus, there are indications that the GBs can act as performance limiting defects in some cases, but the reasons are not fully understood. The motivation for our work is to address why and how it might be possible that only some GBs can degrade the SRF cavity performance.

Our earlier magneto-optical (MO) imaging studies of Nb bi-crystals [20, 21] showed that a GB could preferentially admit magnetic flux with respect to the grains on either side. When such flux penetration occurred, we found that this behavior occurred whether we had performed electropolishing (EP), buffered chemical polishing (BCP), or even just mechanical flattening. However, preferential flux penetration along GB did not occur when the GB plane was significantly tilted with respect to the external field, H_{ext}. An important feature of the SRF cavities is that the RF current flows only within a surface layer that is a penetration depth $\lambda \sim$ 40–50 nm thick, a realization that has generated intense effort to understand and to perfect this surface layer [4]. It is clear that polishing by BCP or EP makes huge changes to the surface roughness, chemistry, and ultimate the SRF cavity performance in some ways that are not yet fully understood. The fact that baking at ~120 °C/48 h, ~600 °C/10 h or 800 °C/2 h after chemical polishing, or recent N_2 doping [22] or N_2 infusion [23] strongly affect the SRF performance makes it clear that diffusion and redistribution of light elements like O, N, and H can play important roles in determining the local properties of 1D or 2D defects like vacancies, dislocations and GBs [7].

Our earlier MO imaging results suggest a parallel with the intrinsic weak link behavior of GBs in the high temperature cuprate superconductors (HTS) [24, 25]. However, superconducting properties of a conventional low temperature superconductor like Nb are much less sensitive to the typical materials defects compared to HTS cuprates which have much lower carrier density and much shorter coherence lengths ($\xi_{Nb} \approx 40$ nm versus $\xi_{HTS} \approx$ 1–2 nm). Unlike HTS, the GB problem in Nb is not intrinsic but may result from such extrinsic factors as contamination of the GBs during cavity processing. Moreover, the current-blocking effect of a GB can depend on its relative orientations with respect to the RF magnetic field and current. Previous investigations of vortex pinning in Nb bi-crystals [26, 27] showed that the critical current, I_c, was significantly enhanced by the interaction of vortices with the GB plane if it was aligned parallel to the external field. In this case, vortices were pushed against the GB by the Lorentz force so that I_c was enhanced. However, if current crosses the GBs, I_c could be diminished if the superfluid density at the GB is reduced.

The possibility of the SRF performance degradation in the Nb cavity due to significant variation of GB properties produced by very different chemical treatments during cavity fabrication has motivated the experiments described here. In this work, we investigated the dc magneto-transport properties of a single GB cut from a large-grain ingot slice of SRF-quality Nb from which high gradient cavities had been made.

2. Experiment

2.1. Sample description

We used single- and bi-crystals cut from a very large-grain (grain size > ~5–10 cm), quasi-single crystal ingot (~30 cm in diameter) manufactured by CBMM [2]. The ingot has a high purity, as indicated by an RRR > 250. It was supplied to us by Kneisel and co-workers at Thomas Jefferson National Accelerator Facility (TJANF or JLAB). JLAB fabricated two superconducting cavities with such large-grain Nb ingot slices. After final fabrication with a BCP process, the cavities showed an excellent accelerating gradient of ~45 MV m^{-1} at 2 K [1].

To investigate the GB properties, we compared the DC transport electromagnetic properties of single- and bi-crystals cut from the same Nb slice used in the previous work [20, 21]. Figure 1(a) shows a schematic of the ingot slice and the GB region used for this study. This image was constructed by superimposing top and bottom images. A 'thick' GB implies a tilted (≫15°) GB plane while a 'thin' GB has a GB plane mostly perpendicular to the surface. Multiple I-shaped (dog-bone) samples were cut from the slice by electrical discharge machining (EDM). Single crystals were cut out from a large central grain (grain size ≫ 10 cm), while bi-crystals were cut from the region, indicated by the blue-dotted rectangles in figure 1(a). This bi-crystal has a crystallographic misorientation of ~26° across a relatively straight and long (>5 cm) GB plane, thus allowing preparation of several bi-crystals with the same crystal misorientation. After cutting, all sample surfaces were mildly treated by BCP in order to remove ~20–30 μm depth of surface damaged by the EDM cutting.

The samples for transport V–I measurement had to be made as thin as possible in order to reduce I_c because of the

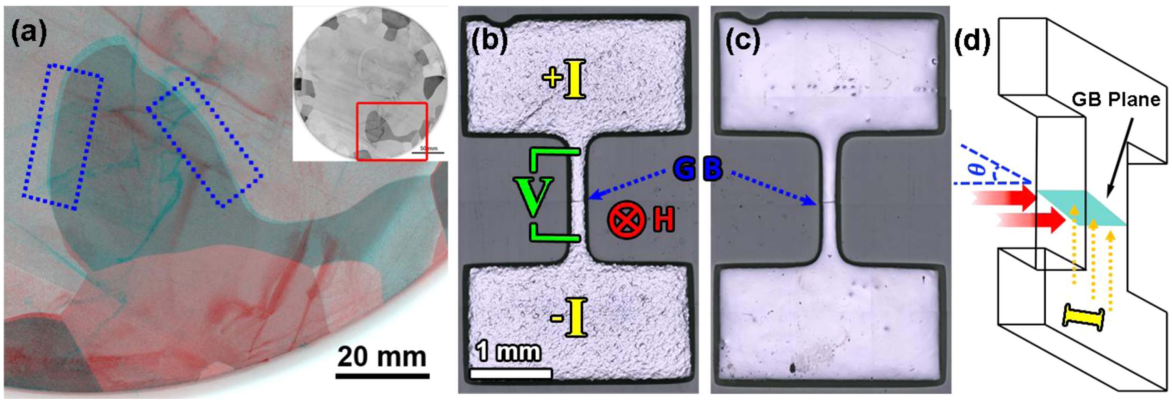

Figure 1. (a) Overview of the large-grain (grain size > ∼5–10 cm), high purity (RRR ⩾ 250) niobium ingot slice (2.5 mm thickness), provided by the Thomas Jefferson National Accelerator Facility (TJNAF) for this study. (b) The top and (c) bottom surface view of an I-shape (dog-bone) bi-crystal sample used for DC transport measurement after ∼50 μm layer removal with BCP. The GB groove indicated by blue-dotted arrows in (b) and (c) appeared after BCP. (d) Schematic diagram of the angular direction (θ) between applied magnetic field (H) and the plane of GB and the direction of the transport current (I) on the I-shape sample. This bi-crystal sample was extracted from the regions indicated by the dotted blue rectangles in (a). The disorientation angle of the GB plane to the surface is ∼5° and the crystallographic misorientation across the GB is ∼26°.

difficulty in making low-resistance joints to Nb. A thin sample is also advantageous because high purity Nb is a marginal type II superconductor with only small difference between its lower critical field, H_{c1} (4.2 K) ≈ 180 mT, and critical field, H_c (4.2 K) ≈ 200 mT [28]. Thinning the sample produces a large demagnetizing factor (D_z) for field perpendicular to the flat sample, causing vortex penetration to occur at H_{ext} values significantly lower than H_{c1}. In this way we were able to access a much larger field range in which vortices were present so as to distinguish between intra- and inter-grain V–I characteristics. We also wanted to make all sample surfaces as representative as possible of an actual fabricated SRF Nb cavity surface by using typical cavity surface treatments like BCP and EP, while minimizing the introduction of impurities and mechanical damage to the high purity and soft Nb. The sample were prepared as described below.

(1) I-shaped single- and bi-crystals were prepared by mechanically grinding away from the bottom surface to ∼150–200 μm thickness, while leaving the top surface in the as-received condition. We used a special metallographic technique that we developed to minimize damage to the Nb surface [29].
(2) The ground (bottom) surface was ultra-finely polished with 0.05 μm colloidal silica for ∼12–24 h by a vibratory polisher [30] in order to minimize surface defects which might induce local corrosive reactions during later chemical treatments and to remove surface mechanical damage introduced in step 1.
(3) All surfaces were finalized with either BCP or EP treatments to produce clean, damage-free surfaces representative of a typical SRF Nb cavity. In BCP process, the samples were chemically treated with a mixed solution of hydrofluoric acid (HF, 49.5%), nitric acid (HNO_3, 69.5%), and orthophosphoric acid (H_3PO_4, 85%) in a 1:1:2 volumetric ratio at 10 °C–20 °C for 20–70 min. For EP treatments, I-shape bi-crystals were electropolished at 12 V, for 1.2–1.5 h after the mechanical thinning (steps 1 and 2). These BCP and EP treatments further reduced the sample thickness by up to ∼80–100 μm.
(4) The bridge thicknesses of some single- and bi-crystal samples were further reduced with extra BCP treatments in order to minimize I_c. For this secondary BCP procedure, the I-shaped samples were glued on a sapphire (Al_2O_3) plate with GE varnish and the two current contacts at the ends of the 'I' were wrapped with polytetrafluoroethylene (PTFE) tape to prevent excess thinning during the second BCP.
(5) To further investigate whether GB grooves produced during BCP treatments have any effect on the measured V–I characteristics, an artificial groove was cut in a single crystal using a focused ion beam (FIB). In parallel with this FIB-made groove, an initially tested BCP'ed bi-crystal was re-measured after removing the BCP-made groove by mechanical polishing using 6 and 1 μm diamond and 0.05 μm colloidal silica on a vibratory polisher.

Figures 1(b) and (c) show both top and bottom surface images of an I-shaped (dog-bone) bi-crystal sample after step 3. Surface, GB topological features, and dimensions of the samples prepared for the DC transport characterization were evaluated by scanning laser confocal microscopy and are listed in table 1. We found that BCP produced a deep (∼4–7 μm) and highly-inclined GB groove. In contrast, much shallower (∼0.3–0.5 μm) and narrower (∼0.5–2 μm) GB grooves were formed by EP.

2.2. DC field transport V–I characterizations

We employed the same transport current characterization method used earlier for exploring the properties of low angle grain boundaries in HTS YBCO thin film bi-crystals [24, 25]. The external magnetic field (H_{ext}) was applied parallel to the

Table 1. Samples examined in transport *V–I* characterizations. Note that the disorientation angle ∼5° is the angle between the surface normal and the GB plane. For comparison, the aspect ratio of the 7° [001] tilt thin film (LAGB: low angle grain boundary) HTS $YBa_2Cu_3O_{7-\delta}$ bi-crystal used to develop the AJ flux flow model [23] is 96, much larger than the 5–16 possible here.

Sample ID[i]	Sample type (misorientation angle[ii])	Surface treatments	Surface topological features	Aspect ratio (width (w) to thickness (t) ratio (μm))
SC1	Single crystal	1st BCP (∼40–50 min) and 2nd BCP (∼70 min, at ∼ 20 °C)	∼0.5–2.0 μm roughness	5.4 (315.3/58.6)
SC2	Single crystal	1st BCP (∼40–50 min) and 2nd FIB grooving	Artificially grooved (∼10–15 μm depth) in the middle of the bridge	4.6 (557.5/121.1)
BC1	Bi-crystal (∼26°)	1st BCP (∼40–50 min) and 2nd BCP (∼70 min, at ∼20 °C)	Deep (∼3–5 μm) and highly-inclined GB groove	7.2 (331.9/46.3)
BC2	Bi-crystal (∼26°)	1st BCP (∼40–50 min) and 2nd BCP (∼70 min, at ∼20 °C)	Deep (∼3–5 μm) and highly-inclined GB groove	12.5 (603.93/50.12)
BC3	Bi-crystal (∼26°)	EP (12 V, ∼1.2 h)	Uniform surface and shallow (∼0.3 to 0.5 μm) GB groove	7.0 (730.9/104.3)
BC4	Bi-crystal (∼26°)	1st BCP (∼10–20 min) and 2nd mechanically polishing	Flat surface ($\ll$0.1 μm roughness)	16.0 (742.0/46.5)

[i] SC and BC stand for single and bi-crystal, respectively.
[ii] The misorientation angle is the crystallographic misorientation angle between the two grains.

straight GB plane of our bi-crystals, while the transport current flowed perpendicular to the GB plane, as illustrated in figure 1(d), where θ is the angle between the applied magnet field and the GB plane. In this geometry, the Lorentz force is parallel to the GB plane, allowing us to reveal any tendency for weak superconductivity at the GB. To supplement our earlier MO study [20, 21], we also rotated the GB plane relative to H_{ext}. For this DC transport characterization, we used a 1 T (Tesla) electro-magnet having very low remnant field (1–5 Oe) in order to avoid concerns about the effect of remnant fields on the *V–I* responses. Although our Nb samples were thinned down to the order of 10 μm, I_c was still rather high, so to avoid heating at the current joints we measured the *V–I* curves in DC mode at 1 mA $< I <$ 0.5 A and in pulsed mode at higher currents 0.5 A $< I <$ 1.5 A. All measurements were performed at 4.2 K in a liquid helium bath to ensure maximum cooling.

3. Results

Voltage–current density characteristics of the BCP-treated single and bi-crystal samples are shown in figure 2 in both linear (a), (b) and log–log (c), (d) coordinates. The *V–J* curves of the BCP'ed single crystal show a typical flux flow behavior, except for the highest I_c log–*V* log transitions found at the lowest test field of 50 mT, where we believe some current transfer resistance is present. At higher H_{ext}, both sets of *V–I* characteristics of the single crystal show a smooth and progressive increase in voltage as current is increased above I_c. This behavior indicates no preferential flux flow channels in the single crystal. In contrast, the bi-crystal (figures 2(b) and (d)) shows a distinctly bimodal resistive behavior. In log–log coordinates, the *V–J* curves are single crystal-like for $H_{ext} < 80$ mT, but for $H_{ext} \geqslant 80$ mT they show a marked change, now exhibiting clear evidence of a resistive transition at a much lower critical current I_b than I_c in the grains on either side of the GB. As the current is raised, *V* rises much less steeply than for the single crystal in figures 2(a) and (c), transitioning smoothly to the single crystal characteristics at higher *V* and *J*. The lower voltage transition is quasi-linear, as shown in figure 2(b). At $H_{ext} \geqslant 80$ mT, the *V* response starts to show a linear dependence. $H_{ext} = 80$ mT corresponds to the onset of preferential GB flux flow at much lower currents than which causes vortex motion within the grains on either side of the GB. These characteristics show that inter-granular critical current, I_b is well below I_c in the grains. The displaced ohmic behavior $V = (I - I_b) \cdot R$ at $I \approx I_b$ defines the excess GB resistance $R(H)$ [24].

Because, in general, EP-treated polycrystalline cavities are superior to BCP'ed cavities [3, 4, 31], we also compared the transport *V–J* characteristics of an EP'ed bi-crystal (BC3) with that of a BCP'ed bi-crystal (BC1). This EP'ed bi-crystal was extracted from the GB region indicated in figure 1(a). It had a relatively narrow (~0.5–1 μm) and shallow (~0.3–0.5 μm) GB groove compared to the BCP'ed bi-crystal (BC1), as detailed in table 1. The *V–J* characteristics of the EP'ed bi-crystal are shown in figure 3. In contrast to the BCP'ed bi-crystal in figures 2(b) and (d), this EP'ed bi-crystal showed no discernable preferential GB flux flow behavior in either log–log or linear scale coordinates. In fact, the *V–I* characteristics of EP'ed bi-crystals are rather similar to those of the BCP'ed single crystal. However, some indications of preferential GB flux flow are observable at low transport currents for fields $\leqslant$100 mT in the linear *V–I* coordinates (figure 3(a)), and for fields $\geqslant$130 mT in the log–log coordinates (figure 3(b)). Nevertheless, the dissipation is obviously much smaller than in the BCP'ed case.

To understand whether the large GB groove developed by the BCP facilitates the GB flux flow, we explored the transport characteristics of (1) an artificially grooved BCP'ed single crystal (SC2) by trenching the top and bottom surfaces with a Ga FIB after the final BCP treatment, and (2) a mechanically flattened bi-crystal (BC4), in which the top and bottom surfaces groove produced by the BCP treatment were completely smeared away by ultra-fine mechanical polishing. We used a 557 μm (*w*) $\times$ 59 μm (*t*) BCP-treated single crystal. A focused heavy Ga ion beam could damage the surface microstructure of the niobium, thus we followed the same delicate FIB procedure developed for transmission electron microscopy (TEM) sample preparation [29] in order to minimize damage. The *V–J* characteristics of these two samples are shown in figures 4 (SC2) and 5 (BC4), respectively. In the case of the grooved single crystal (SC2), transport superconducting properties in fields up to 150 mT were not depressed by the artificial groove. However, at higher fields ($H_{ext} \geqslant$ 200 mT, H_c (Nb) is ~180–200 mT at 4.2 K [28]), there was an ohmic component to the behavior, which suggests that vortex flow appeared at the necked region of smaller cross-section (~10% of width and ~25% of thickness reduction) produced by FIB milling. We interpret this crossover behavior as occurring by additional vortex pinning induced by Ga^+ ion radiation damage at lower fields.

As a second test of the influence of grooving, figure 5 shows that GB flux flow is still very evident even after the GB groove was completely removed by mechanical polishing (BC4). The quasi-linear *V–J* characteristics in the linear coordinates again indicate preferential GB flux flow of vortices, similar to those in the BCP'ed state (BC1) in figure 2. The results of these two experiments suggest that variations of local topology or grooving are not the prime reason for preferential GB flux flow.

To study the angular dependence of preferential GB flux penetration observed in the earlier MO work [20, 21], the *V–J* characteristics of the BCP'ed bi-crystal (BC2) and the mechanically smoothed bi-crystal (BC4) were evaluated by rotating the GB plane with $\theta = 0°$, 30°, and 60° at $H_{ext} = 80$, 150, and 230 mT, respectively. Figure 6 shows that the GB flux flow dissipation is clearly greatest when the GB plane and H_{ext} are parallel ($\theta = 0°$), but the voltage is markedly reduced as the angle θ increases. This GB effect is more prominent in the smooth-polished bi-crystal. At $H_{ext} =$ 80 mT, in the case of the BCP'ed bi-crystal sample (BC2), the pronounced GB flux flow almost disappeared when H_{ext} was tilted ~30° away from the GB, but, for the mechanically smoothed bi-crystal, the GB dissipation disappeared only for

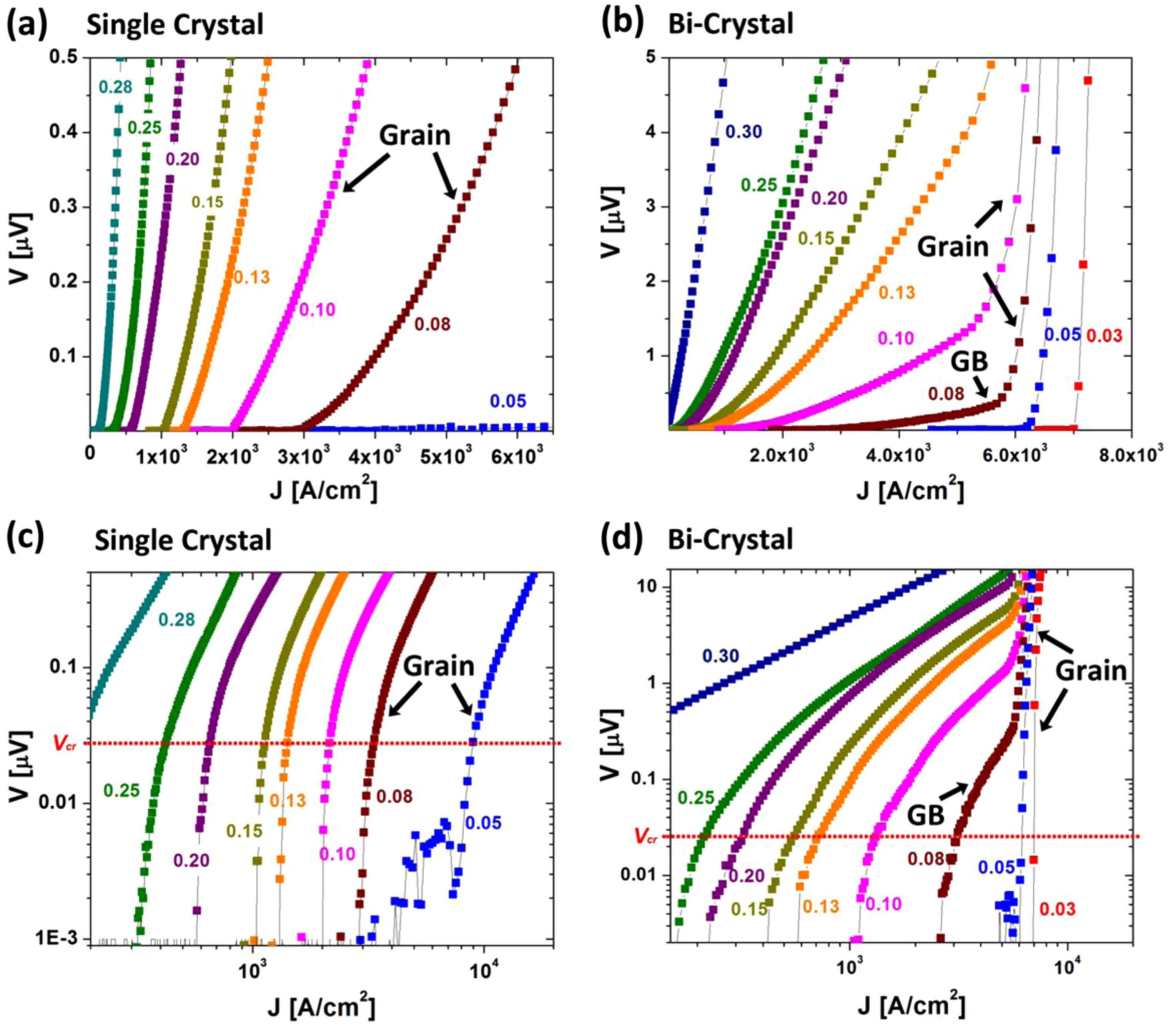

Figure 2. *V–J* characteristics at 4.2 K of the BCP'ed single crystal (SC1) plotted in (a) linear and (c) log–log scales compared to the BCP'ed bi-crystal (BC1) in (b) linear and (d) log–log scales when the external magnetic field is applied normal to the surface plane. The number adjacent to each curve represents external magnetic field (Tesla). Since the BCP'ed bi-crystal has ∼5° of disorientation between the GB plane and the surface normal, the external magnetic field is slightly tilted to lie very close to the grain boundary plane ($\theta = 0$). The horizontal red-dotted lines in (a) and (d) indicate the voltage criteria (0.1 μV cm^{-1}) used to define $J_c(H)$ in the single and bi-crystals in figure 7.

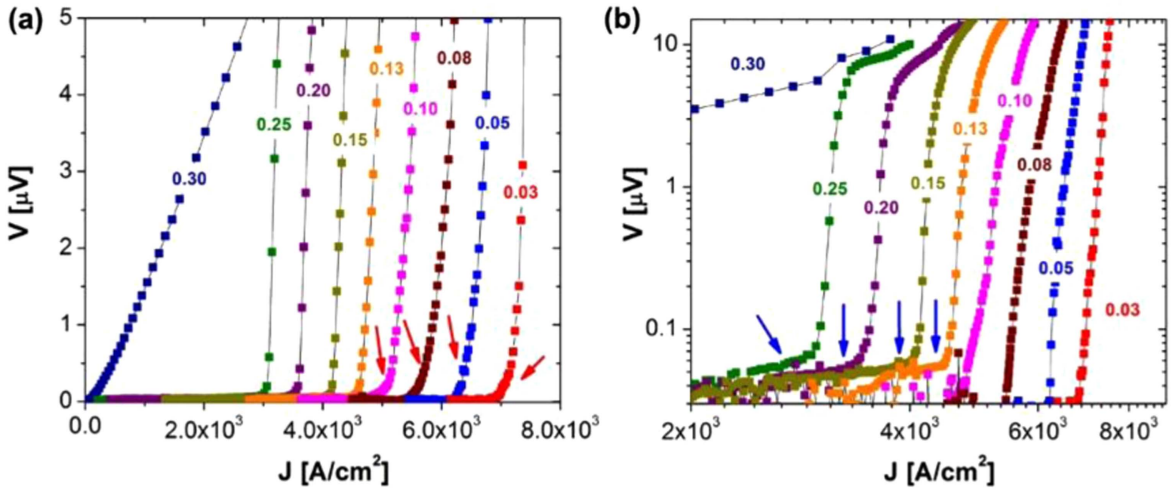

Figure 3. *V–J* characteristics of EP'ed bi-crystal (BC3) in (a) linear and (b) log–log scales at 4.2 K; the red and blue arrows in (a) and (b) indicate possible excess GB resistance, suggesting a vortex flow transition from GB to grains. The inset number gives the magnetic field in Tesla of each curve.

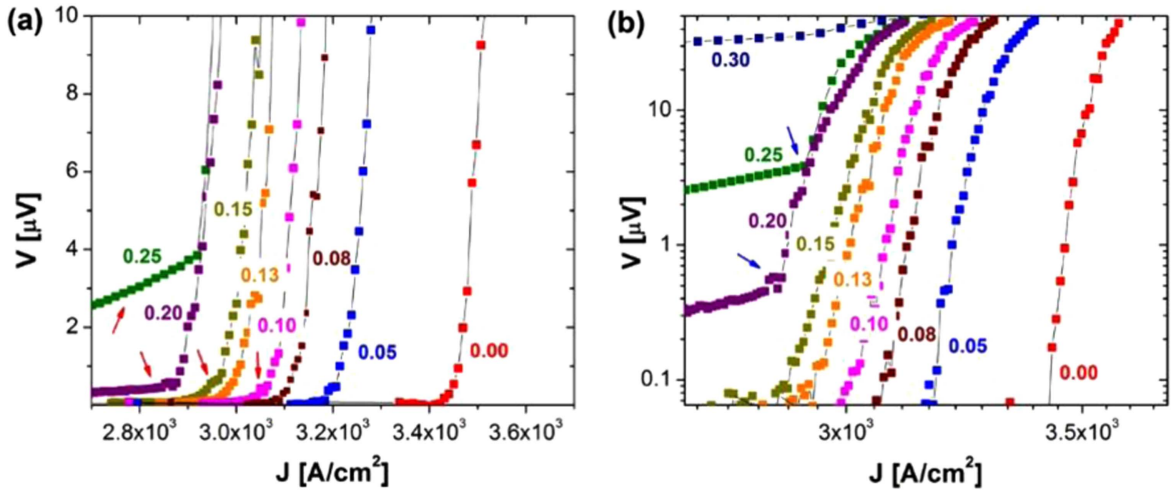

Figure 4. *V–J* characteristics at 4.2 K of the artificially grooved BCP'ed single crystal (SC2) produced by FIB (focused ion beam) in (a) linear and (b) log–log coordinates. The red and blue arrows indicate possible linear flux flow or kinks due to excess resistivity at the groove. The inset number represents the external magnetic field (Tesla).

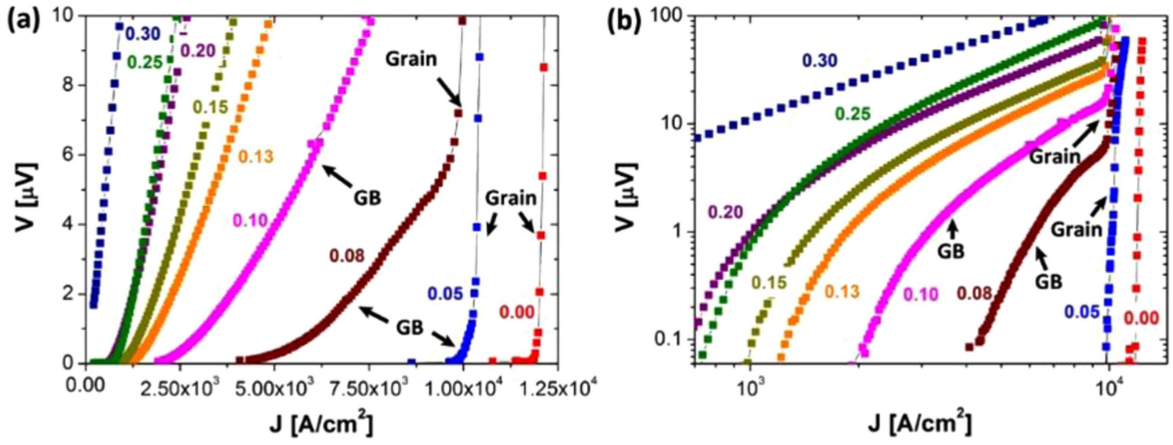

Figure 5. *V–J* characteristics of the mechanically smoothed bi-crystal (BC4) in (a) linear and (b) log–log scale at 4.2 K. The quasi-linearities in (a) are very similar to those of the BCP'ed bi-crystal (BC1) shown in figure 2(b)). The inset number represents external magnetic field (Tesla).

a 60° tilt angle. It was also found that the intra-grain J_c is nearly doubled by the mechanical polishing. A similar tendency is seen for $H_{ext} > H_{c1}$ (≈120 mT at 4.2 K) in figures 6(b) and (d). For instance, the 60° misaligned J_c value when the GB is not limiting I_c is about twice as high as for the polished bi-crystal. It is likely that one reason for this is the surface damage introduced by mechanical polishing that introduces high density of dislocations, enhancing vortex pinning at the GB.

4. Discussion

In this study we measured the influence of a grain boundary of high misorientation angle (∼26°), extracted from SRF-quality Nb ingot slice [1, 2], on the DC transport properties. Direct transport *V–J* characterizations showed that the GB goes into flux flow before the grains on either side do when the magnetic field is nearly parallel the GB plane. This preferential GB flux flow shows a quasi-linear *V–I* characteristic and a distinct kink in the log–log scale *V–J* plot, as is clearly shown in figure 2. GB flux flow is much more substantial in BCP'ed than EP'ed bi-crystals, indicating that grain boundary damage is greater after BCP than after EP treatments. Moreover, the dependence of the appearance of the onset of flux flow at GB on the angle between the magnetic field and the GB plane may indicate why there is no simple correlation between the single GB results presented here and SRF cavity performance.

The field-dependent critical current densities, $J_c(H)$, of the samples studied are compared in figure 7. As marked in figures 2(c) and (d), $J_c(H)$ is defined with an 0.1 μV cm^{-1} electric field criterion and is very sensitive to the appearance of excess GB resistivity. The shape of all $J_c(H)$ characteristics are very similar to each other, except for the FIB'ed single crystal. The inset represents the normalized ratio of $J_c(H)$ of the samples with the BCP'ed single crystal (SC1). It is clearly seen that $J_c(H)$ of the FIB'ed single crystal rapidly increases for $H_{ext} \geqslant 0.1$ T, indicating that the FIB milling significantly enhanced vortex pinning. However, as expected, $J_c(H)$ of the

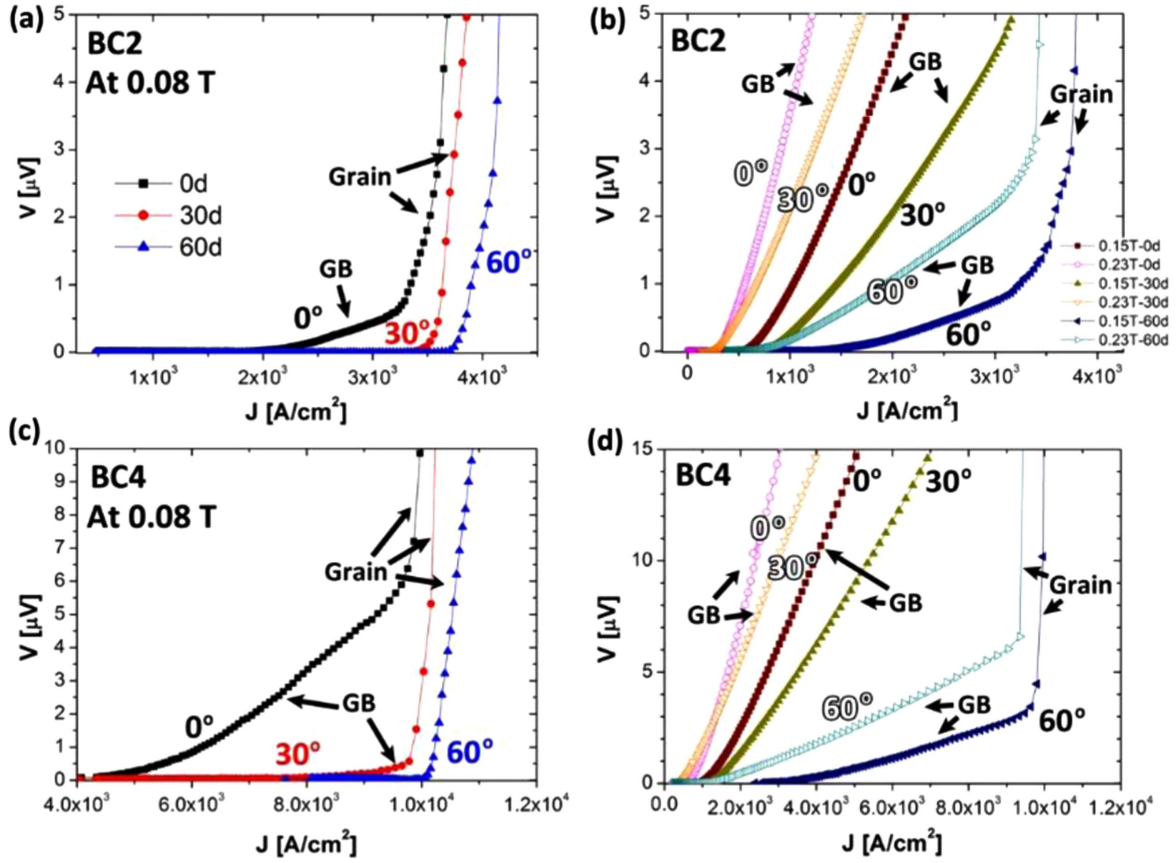

Figure 6. Angular dependent *V*–*J* characteristics of (a) and (b) the BCP'ed bi-crystal (BC2) and (c) and (d) the mechanically flattened bi-crystal (BC4) at 4.2 K with $H_{ext} = 0.08$ T, 0.15 T, and 0.23 T, respectively. The numbers on the plots indicate the misalignment angle (θ) between the GB plane and the vector of applied magnetic field. The solid and outline numbers in (b) and (d) represent the misaligned angles at 0.15 T and 0.23 T, respectively.

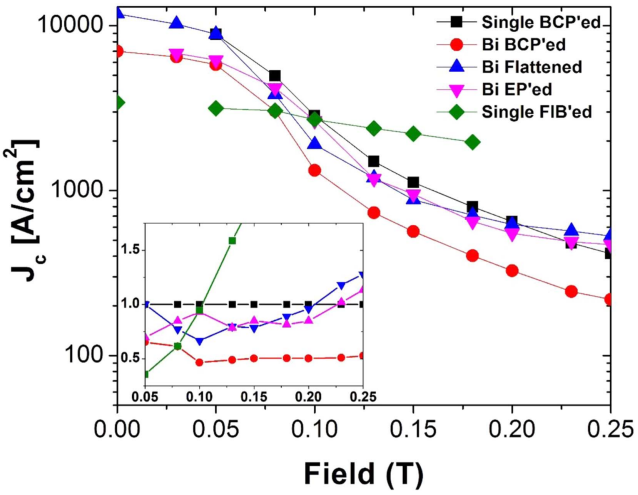

Figure 7. $J_c(H)$ of all samples, in log-linear coordinates. The critical current density, J_c, was determined at, 0.1 μV cm^{-1}, as shown in figure 2. The inset represents normalized $J_c(H)$ characteristics compared to the BCP'ed single crystal (SC1). The anomalous behavior of the FIB'ed single crystal is clear.

BCP'ed bi-crystal (BC1) is markedly lower than for the BCP'ed single crystal (SC1), the $J_c(H)$ difference between them being 2 to 3 after the onset field of GB flux flow, $H_{ext} = 80$ mT. Most importantly, the EP'ed bi-crystal (BC3) always shows higher $J_c(H)$, compared to the BCP'ed bi-crystal (BC1), especially for $H_{ext} \geqslant 0.2$ T. However, this EP'ed bi-crystal show slightly lower $J_c(H)$ than for the flattened bi-crystal (BC4). This suggests that bulk vortex pinning is enhanced by mechanical polishing damage, and also that, unlike BCP, the EP process can efficiently remove the Nb surface without a significant negative effect on the GB. The $J_c(H)$ comparison shows that variations in bulk superconductivity of SRF Nb are highly dependent on the specifics of the surface treatment.

In these DC experiments, the entire GB plane contributes to the flux flow, unlike the RF supercurrents flowing only within the penetration depth, $\lambda \approx \sim$40–50 nm at the cavity surface. Thus only a 50–100 nm portion of the whole GB plane may contribute to the $Q(H)$ curve of the SRF Nb cavities. The single cell SRF Nb cavities [1] fabricated at TJNAF show high accelerating gradient approaching the theoretical limit (50 MV m^{-1}) after a BCP process in combination with post ~120 °C bake. Intrinsic high material property, RRR $\geqslant$ 250, and cutting-edge surface preparations could sustain BCS surface superconductivity close to the theoretical field limit, $H_{RF} \approx 200$ mT, and further reduce the surface resistance. However, these TJNAF cavities, even the recently fabricated EP'ed cavities with large-grain Nb ingot slices (RRR $\geqslant$ 200) [32], have high-field $Q(H)$ slope at $H_{RF} \approx$ 120–150 mT.

Although several mechanisms of surface superconductivity breakdown such as oxidization, flux trapping, and lossy $Nb_{1-x}H_x$ precipitation have been widely discussed, our DC transport study suggests that GBs could be another contributor to performance degradation related to HFQS. Our study suggests that GB degradation most likely occurs at GBs that have a planar alignment within the top surface sheath of 50–100 nm, that is very close to parallel to the external magnetic field can fully lie. Such sub-surface GB plane segments would not be observable by optical examination of the cavity surface [18]. An extensive study of texture behavior [33] on SRF-quality Nb materials indicates strong development of preferred grain orientation based on cold work deformation, leading to enhancement of mechanical property. However, variation of Nb grain boundary planes with respect to cold work deformation has not been substantially explored yet.

In the same context of HTS YBCO GB properties [24, 34, 35], we believe that two factors are responsible for the marked angular behavior shown in figure 6. One is the fact that when the external field is applied to a tilted or meandered GB plane, vortex segments at GBs cannot move under the action of the Lorentz force without pulling the generally stronger pinned vortex segments than in the grains or cutting and reconnecting the neighboring flux line. Another contributing factor may be the increasing area of GB for tilted or meandered GBs for transport currents by simple geometrical considerations.

From the DC transport characteristics, it is evident that the BCP treatment produced more weakly-coupled GBs as compared to the EP. EP is now the preferred route for producing reproducible high performance in SRF cavities [4, 31] for better surface topography and weaker grooving at GBs. However, our study has shown no significant influence of grooving on the GB flux flow (see figures 4 and 5). Thus, the chemistry and morphology of impurities segregated at the GBs induced by surface chemical treatments are likely the essential factors which contribute to the GB degradation, leading to preferential GB flux flow. A recent surface susceptibility study [36] showed that BCP can contaminate the GBs more than EP if cold work deformation of an intermediate strain level ($\varepsilon > \sim 4\%$) is applied. In this long-range strain, high density of dislocation networks piled up at GBs or isolated dislocation cell structures or faceting may result in Cottrell atmosphere of segregated impurities during chemical treatments, which in turn cause local weakening of superconductivity along GBs [37]. A cross-section microstructural study by high resolution TEM [29] showed that BCP preferentially oxidizes the GB region of a Nb bi-crystal from a large-grain ingot slice [38]. However, the thin TEM film of Nb bi-crystals studied in [29] had severe dislocation-decorated GB structures just after initial thinning, so there might remain some amount of dislocation networks at GB. In contrast, Trenikhina [39] did not observe any GB oxidation at a hot spot region cut out from a thermometry-tested polycrystalline EP'ed cavity. Therefore the difference in crystallographic and texture properties between large or fine grain Nb materials [40] may lead to different GB properties in both TEM studies, although the mechanism by which different chemical treatments affect current transport through GBs have not been well understood. Impurity segregation at GBs in metallic materials with solute atoms like C, N, O, H, can be dependent on GB misorientation angle between neighboring grains [41]. One can assume that the preferential flux flow along GBs in the Nb cavities result from lattice disturbance at GB with dislocations due to mechanical deformation and segregation of impurities during surface chemical treatments. In addition, our observation that the inter-grain J_b caused by pinning of vortices along GB depends on chemical treatments indicates that these treatments during the cavity fabrication process introduce structure defects, size of the order of the coherence length, $\xi_{Nb} \approx 50$ nm. Such defects could be oxides and hydrides precipitates at dislocation networks or dislocation cells near GBs.

The kinks on the V–J curves at $J_b < J < J_c$ observed on the BCP'ed bi-crystals are indicative of channel flux flow of vortex row along GBs [25, 37]. The width W of such channel and the number of moving vortex rows N_{row} can be evaluated from the following expression for the flux flow resistance R_f:

$$R_f(H) = \frac{\rho_n \times W(H, J) \times H}{H_{c2} \times A}, \tag{1}$$

$$N_{row} = \frac{W}{a} = W\sqrt{\frac{B}{\Phi_0}}. \tag{2}$$

Here H_{c2} is the upper critical field, A is the cross-sectional area, and $a = \sim(\Phi_0/B)^{1/2}$ is the intervortex spacing and Φ_0 is the flux quantum. Taking $\rho_n = 1.46 \times 10^{-7}$ ohm m and $B_{c2} = 450$ mT for the BCP'ed bi-crystal at $H_{ext} = 80$ mT we obtained $W \cong 0.185$ μm and 0.5 μm corresponding to $N_{row} \cong 1.15$ and 3 for the low and high V portion of the V–I curve, respectively. This rough estimate indicates that the initial GB flux flow first arises at $J \approx J_b$ from depinning of a single row of vortices, which then transitions to multiple rows at higher voltages at which GB vortices starts dragging neighboring rows of intra-grain vortices. These effects have been studied extensively for GBs in HTS cuprates, particularly YBCO bi-crystals [12, 25]. In fact, vortices moving along strongly-coupled GBs (which are of prime interest for the SRF cavities) are mixed Abrikosov–Josephson vortices for which the flux flow resistance is given by [25]

$$R_f = \frac{R\sqrt{B}}{\sqrt{B + B_0}}, \tag{3}$$

$$B_0 = \frac{\Phi_0}{4\pi^2 l^2}, \quad l = \frac{3\frac{3}{2}\xi J_d}{4J_0}, \tag{4}$$

where R is the excess GB resistance in the normal state, l is the length of the Josephson core along GB, J_d is the Ginzburg–Landau depairing current density in the grains, and J_0 is the Josephson current density of the GB. Fitting the observed field dependence $R_f(B)$ with equation (3) allows us, in principle, to extract R and the intrinsic depairing density of J_0 of GB and thus to attest the degree of superconducting coupling across GB and its current transparency, as was done previously for YBCO bi-crystals [25]. However, applying

equation (3) to GBs in Nb turned out to be not so easy, because, unlike YBCO bi-crystals, the *V–I* characteristics of Nb bi-crystals shown in figures 2–6 do not have well-defined linear portions which would allow us to unambiguously extract $R_f(B)$ from the experiment data.

The observed nonlinearity of $V(I)$ in the flux flow region could result from inhomogeneity of transport current and local induction along the grain boundary. One reason for that is that Nb is a marginal type II superconductor for which the flux flow region $H_{c1} < H < H_{c2}$ is rather narrow, particularly in comparison with the HTS cuprates. To widen the flux flow we diminished the perpendicular H_{c1} by reducing the thickness of Nb bi-crystals using both mechanical thinning and the BCP, which can also result in inhomogeneity of the thickness t on the micrometer scale. Our bi-crystals had the final thickness $t = 50$ μm and an aspect ratio = 7–10 (see table 1), resulting in a much lower $B_{c1} = 10$–20 mT than the bulk $B_{c1} \approx 160$–180 mT for Nb at 0 K. However, in the low field region, $B \leqslant B_{c1}$, distribution of the local magnetic induction across a thin film strip can be highly inhomogeneous [42]. To estimate the penetration field for the BCP'ed bi-crystal (BC1), we used two different models depending on the shape of the sample edges, with an aspect ratio $(w/t) = 7.2$, $J_c = 10^8$ A m^{-2} (from figure 7), and $B_{c1} = 150$ mT. For rounded edges, we may use an elliptical approximation of the cross-section, which gives the smallest penetration field:

$$B_{p1} \approx \frac{B_{c1} \cdot t}{w} \approx 21 \text{ mT}. \quad (5)$$

For a rectangular thin film strip, B_p is enhanced by the geometric barrier [42];

$$B_{p2} \approx B_{c1}\sqrt{\frac{t}{w}} \approx 56 \text{ mT}. \quad (6)$$

Both equations (5) and (6) give B_p comparable to the field range in which our transport measurements were performed, so the transport current density flowing across the GB was likely non-uniform. Thus, the conditions under which analysis based on equation (3) is applicable are not satisfied for our BCP'ed bi-crystals. Satisfying these conditions would require much thinner film ($t \ll 10$ μm) with a large high aspect ratio $w/t > 80$. The low energy coaxial energetic deposition technique has been used to successfully fabricate Nb thin films with bulk-like properties on a MgO substrate [43]. Such Nb films would be good candidate for the measurements of the depairing current density at the GB, J_0, using equations (3) and (4) in order to determine the ultimate current limit of polycrystalline Nb. Although we could not extract J_0 in our experiments, our data show that the critical current due to depinning of vortices along GB is smaller in BCP'ed bi-crystals than in EP'ed bi-crystals. This fact may be indicative of weaker coupling across BCP'ed GBs and smaller J_0 which would manifest in a larger Josephson core size l of GB vortices defined by equation (4). In turn, larger core size of GB vortices implies their weaker pinning [44], which results in smaller critical currents in BCP'ed bi-crystals.

5. Conclusion

Our magneto-transport measurements on Nb bi-crystals have shown clear evidence that the grain boundary causes a flux flow channel for a few vortex rows moving though pinned vortices in the grains. This effect of channel flux flow along GBs is most pronounced if the external magnetic field is aligned close to the GB plane and diminishes as the field is tilted away from the GB plane. We also observed that the preferential flux flow along GB is more pronounced for a BCP'ed bi-crystal than for an EP'ed bi-crystal. These results are indicative of weaker superconducting coupling across GBs in BCP'ed bi-crystals which can be essential for the polycrystalline Nb resonator cavities. To obtain ideal performance of SRF Nb cavity, detailed study of microstructural behavior of SRF Nb in conjunction with cold work deformation and surface chemical treatments is highly recommended to minimize grain boundary segregation and rearrangement of grain boundary plane against surface normal.

Acknowledgments

This work was supported by the US DOE under awards DE-FG02-05ER41392, DE-FG02-07ER41451, FNAL PO 570362, and by the State of Florida. The authors would like to thank P Kneisel, G Myneni, G Ciovati, P Dhakal, and colleagues at Thomas Jefferson National Accelerator Laboratory for providing the large-grain high purity Nb slice and fruitful dissuasion. Special thanks to P Bauer and C Antoine for support and valuable discussions at the early stage of this work.

ORCID iDs

Z-H Sung https://orcid.org/0000-0002-5927-1775
P J Lee https://orcid.org/0000-0002-8849-8995

References

[1] Kneisel P, Myneni G R, Ciovati G, Sekutowicz J and Carneiro T 2005 *Proc. Particle Accelerator Conf. (Knoxville, TN)* ed N Holtkamp TPPT076
[2] Kneisel P, Ciovati G, Dhakal P, Saito K, Singer W, Singer X and Myneni G R 2015 *Nucl. Instrum. Methods Phys. Res.* A **774** 133–50
[3] Lilje P *et al* 2004 *Nucl. Instrum. Methods Phys. Res.* A **524** 1–12
[4] Padamsee H, Knobloch J and Hays T 1998 *RF Superconductivity for Particle Accelerators* (New York: Wiley)
[5] Romanenko A and Padamsee H 2010 *Supercond. Sci. Technol.* **23** 045008
[6] Barkov F, Romanenko A, Trenikhina Y and Grassellino A 2013 *J. Appl. Phys.* **114** 164904
[7] Romanenko A, Barkov F, Cooley L D and Grassellino A 2013 *Supercond. Sci. Technol.* **26** 035003

[8] Romanenko A and Goncharova L V 2011 *Supercond. Sci. Technol.* **24** 105017
[9] Ciovati G 2006 *Appl. Phys. Lett.* **89** 022507
[10] Delheusy M *et al* 2008 *Appl. Phys. Lett.* **92** 101911
[11] Dzyuba A and Cooley L D 2010 *Supercond. Sci. Technol.* **23** 125022
[12] Gurevich A and Ciovati G 2008 *Phys. Rev.* B **77** 104501
[13] Ciovati G and Gurevich A 2008 *Phys. Rev. Spec. Top. Accel. Beams* **11** 122001
[14] Bonin B and Safa H 1991 *Supercond. Sci. Technol.* **4** 257
[15] Kneisel P 2003 *Proc. 11th Int. Conf. on RF Superconductivity (Travemünde/Lübeck, Germany)* TuO02
[16] Eremeev G and Padamsee H 2006 *Proc. European Particle Accelerator Conf. (EPAC) (Edinburgh, UK)* MOPCH176
[17] Ciovati G, Kneisel P, Myneni G R and Chattopadhyay S 2006 *Proc. Linear Accelerator Conf. (LINAC) (Knoxville, TN)* TUPO33
[18] Iwashita Y and Tajima Y 2008 *Phys. Rev. Spec. Top. Accel. Beam* **11** 093501
[19] Aderhold S 2011 *Proc. 15th Int. Conf. on RF superconductivity (Chicago, IL)* WEIOB05
[20] Lee P *et al* 2006 *Physica* C **441** 126–9
Myneni G, Carneiro T and Hutton A 2007 *AIP Conf. Proc.* **927** 113–20
[21] Polyanskii A A, Lee P J, Gurevich A, Sung Z-H and Larbalestier D C 2011 *AIP Conf. Proc.* **1352** 186–202
[22] Grassellino A *et al* 2013 *Supercond. Sci. Technol.* **26** 102001
[23] Grassellino A *et al* 2017 *Supercond. Sci. Technol.* **30** 094004
[24] Daniels G A, Gurevich A and Larbalestier D C 2000 *Appl. Phys. Lett.* **77** 20
[25] Gurevich A, Rzchowski M S, Daniels G, Patnaik S, Hinaus B M, Carillo F, Tafuri F and Larbalestier D C 2002 *Phys. Rev. Lett.* **88** 097001
[26] Dasgupta A, Koch C C, Kroeger D M and Chou Y T 1978 *Phil. Mag.* B **38** 367–80
[27] Cai B C, Chou Y T and Dasgupta A 1987 *Phil. Mag.* B **55** 55–66
[28] Saito K 2001 *Proc. 10th Int. Conf. on RF Superconductivity (Tsukuba, Japan)* pp 583–7 PH003
[29] Sung Z-H, Lee P J and Larbalestier D C 2014 *IEEE Trans. Appl. Supercond.* **24** 3
[30] Diaz D J 1987 *Microstruct. Sci.* **14** 489
[31] Saito K 1998 *Part. Accel.* **60** 193–217
Saito K 1997 *Proc. 8th Int. Conf. on RF Superconductivity* vol v1–v4 *(Abano-Teme, Italy)* pp 755–813
[32] Ciovati G, Dhakal P, Kneisel P and Myneni G R 2015 *AIP Conf. Proc.* **1687** 03001
[33] Bieler T R *et al* 2010 *Phys. Rev. Spec. Top. Accel. Beams* **13** 031002
[34] Song X, Daniels G, Feldmann M D, Gurevich A and Larbalestier D 2005 *Nat. Mater.* **4** 470
[35] Feldmann D M *et al* 2007 *J. Appl. Phys.* **102** 083912
[36] Sung Z-H, Dzyuba A, Lee P J, Larbalestier D C and Cooley L D 2015 *Supercond. Sci. Technol.* **28** 075003
[37] Durrell J H, Eom C-B, Gurevich A, Hellstrom E E, Tarantini C, Yamamoto A and Larbalestier D C 2011 *Rep. Prog. Phys.* **74** 124511
[38] Halbritter J 1987 *Appl. Phys.* A **43** 1–28
Halbritter J 2005 *J. Appl. Phys.* **97** 083904
[39] Trenikhina Y, Romanenko A, Kwon J, Zuo J M and Zasadzinski J F 2015 *J. Appl. Phys.* **117** 154507
[40] Flewitt P E J and Wild R K 2011 *Grain Boundaries: Their Microstructure and Chemistry* (New York: Wiley)
[41] Lejček P 2010 *Grain Boundary Segregation in Metals* (*Springer Series in Materials Science* vol 136) (Berlin: Springer)
[42] Brandt E H 1996 *Phys. Rev.* B **54** 6
[43] Krishnan M, Valderrama James C, Zhao X, Spradlin J, Valente Feliciano A-M, Phillips L, Reece C E, Seo K and Sung Z-H 2012 *Phys. Rev. Spec. Top. Accel. Beams* **15** 032001
[44] Gurevich A and Cooley L D 1994 *Phys. Rev.* B **50** 13563